Biophysical Journal, Volume 98

Supporting Material

A Repulsive Electrostatic Mechanism for Protein Export through the Type III Secretion Apparatus

Thenmalarchelvi Rathinavelan, Lingling Zhang, Wendy L. Picking, David D. Weis, Roberto N. De Guzman, and Wonpil Im

Movie Legends

Movie M1. Exportation of MxiH two-helix bundle through the needle channel of *S. flexneri* using SMD. For the sake of clarity, the needle front is not shown. MxiH is colored with blue (N-terminal) to red (C-terminal).

Movie M2. Exportation of MxiH extended alpha helix through the needle channel of *S. flexneri* using SMD. For the sake of clarity, the needle front is not shown. MxiH is colored with blue (N-terminal) to red (C-terminal).

Experimental Methods

Preparation of mxiH mutants for expression in S. flexneri SH116

pRKmxiH containing the *mxiH* gene has been described (1). *mxiH*^{W10} mutants were made by inverse PCR using pRKmxiH as template, a primer composed of GAGAGAGAGGCTCAGCGTXXXATCAT CATTCGGTACTGTAAC where XXX indicates the location of the desired Trp mutation and a primer composed of GAGAGAGAGGCTGAGCTCATTATCTGAAACTTTTGATG (1). The PCR product was digested with BlpI, intramolecularly ligated, and transformed into *E. coli* NovaBlue. The resulting plasmid was electroporated into *S. flexneri* SH116. Ampicillin selection ensured presence of the plasmid while kanamycin resistance and/or Congo red binding indicates presence of the *Shigella* virulence plasmid.

Phenotypic characterization of S. flexneri SH116 expressing different mxiH mutants

The phenotype of each newly generated *mxiH* point mutant strain of *Shigella* was determined by standard assays. *Shigella* invasion functions were tested using a gentamycin protection invasion assay with cultured Henle 407 as described (2). Contact-mediated hemolysis with sheep erythrocytes was used to measure the IpaD-dependent insertion of IpaB and IpaC into target cell membranes as described (2).

References

1. Kenjale, R., J. Wilson, S. F. Zenk, S. Saurya, W. L. Picking, W. D. Picking, and A. Blocker. 2005. The needle component of the type III secreton of *Shigella* regulates the activity of the secretion apparatus. J Biol Chem 280:42929-42937.
2. Picking, W. L., L. Coye, J. C. Osiecki, A. Barnoski Serfis, E. Schaper, and W. D. Picking. 2001. Identification of functional regions within invasion plasmid antigen C (IpaC) of *Shigella flexneri*. Mol Microbiol 39:100-111.

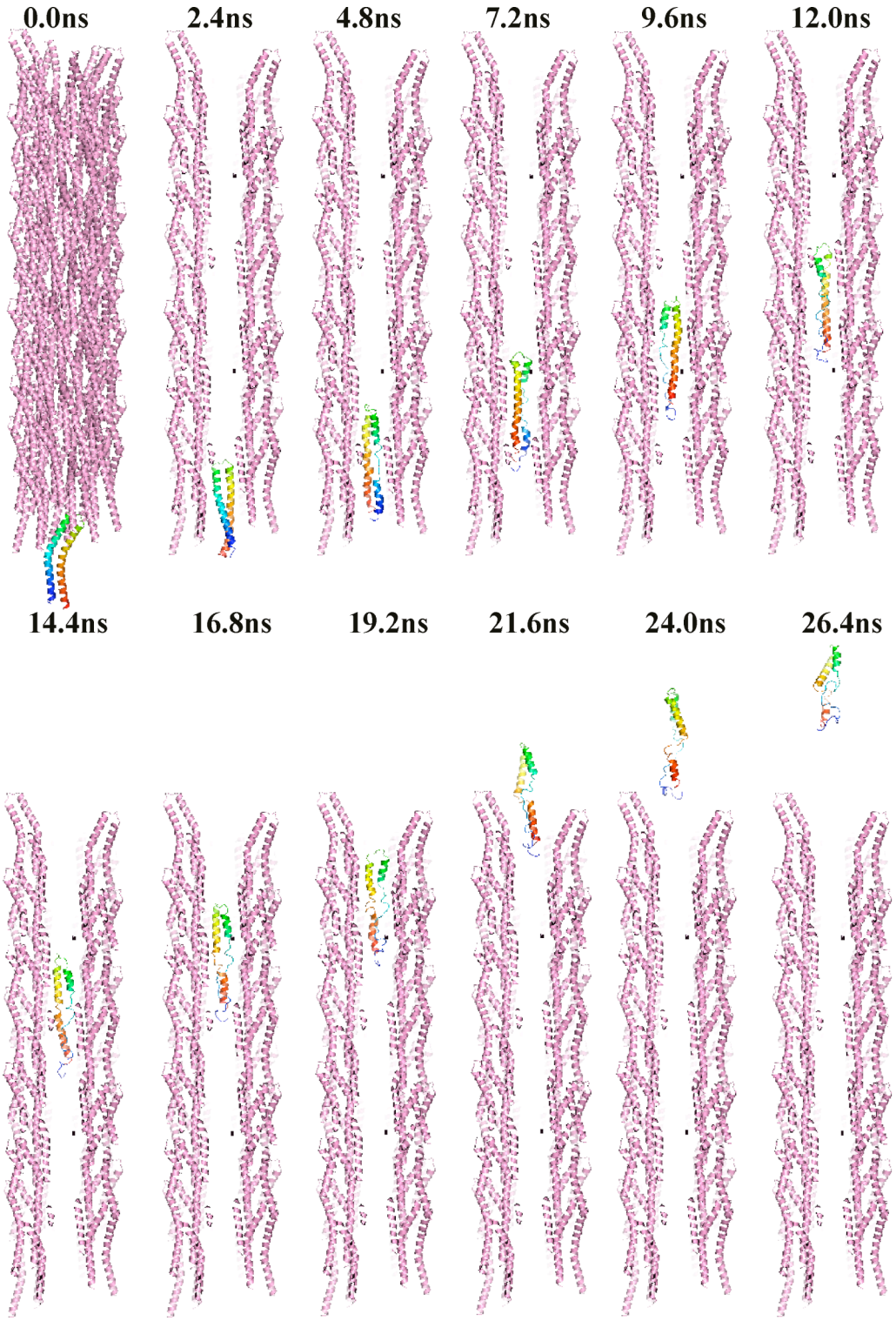

Figure S1. Snapshot showing the transportation of MxiH two-helix bundle across the needle pore. For the sake of clarity, the proteins in the front view are not shown.

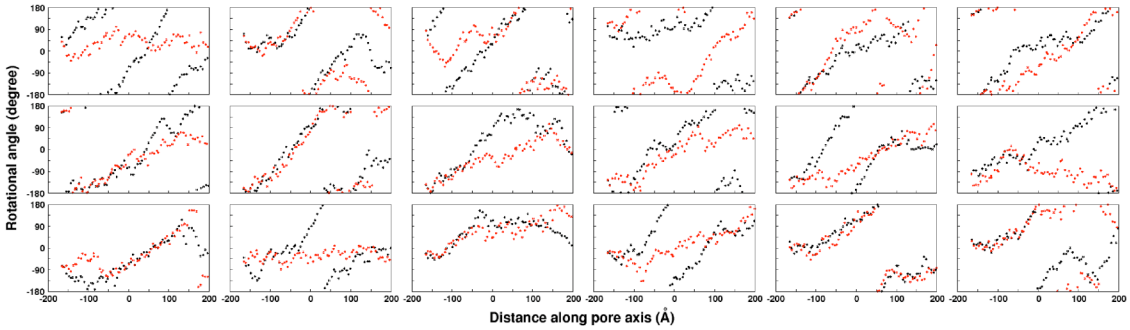

Figure S2 Distance along the pore axis vs rotational angle profile corresponding to W10F (black) and W10Y (red) mutants of two helix bundle with 18 different starting positions.

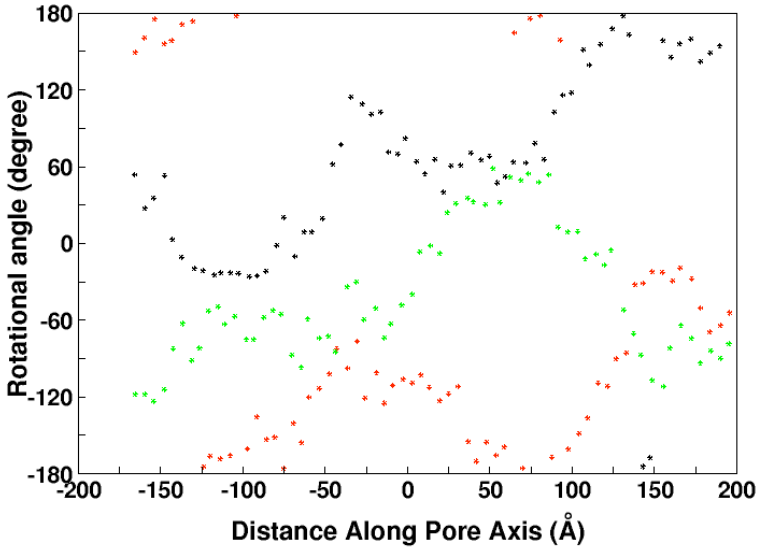

Figure S3 Distance along the pore axis vs rotational angle profile corresponding to 30 Å inner diameter needle with 3 different starting positions: (a) 0° (black), (b) 90° (red) and (c) 180° (green).

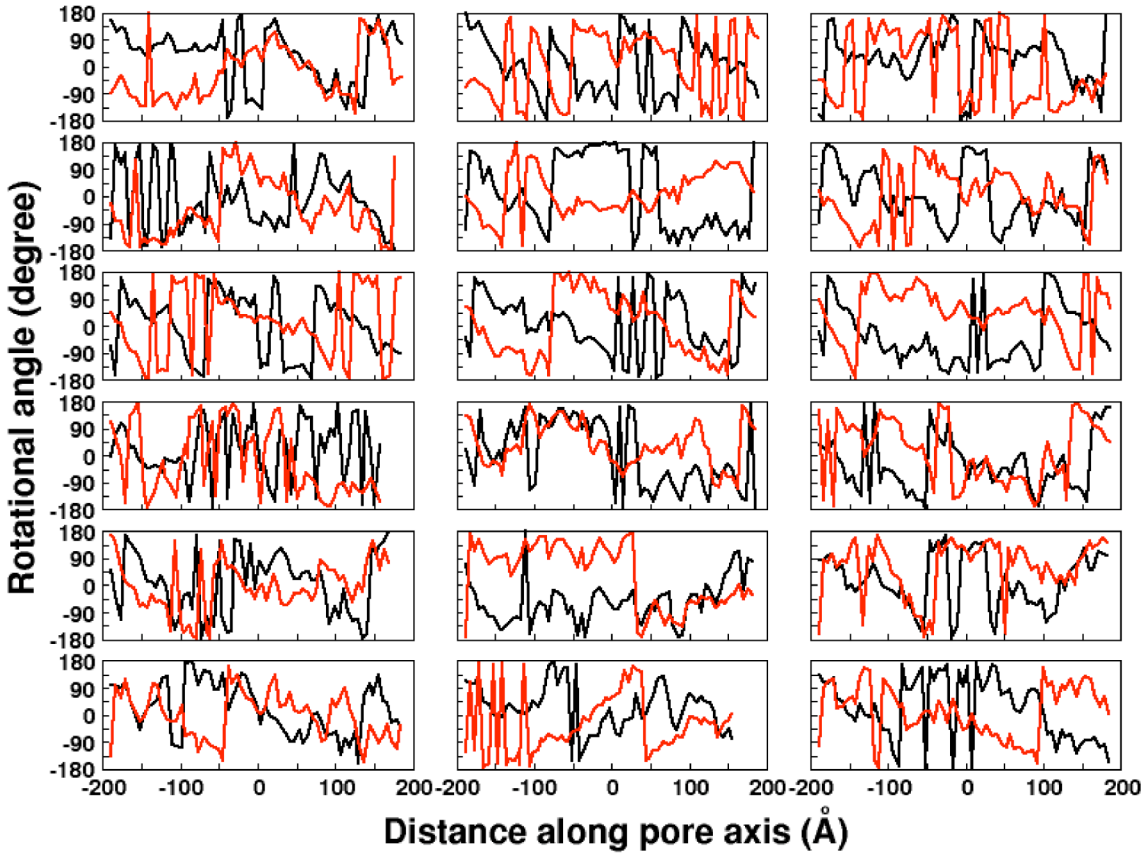

Figure S4 Distance along the pore axis vs rotational angle profile of MxiH straight helix for the regions 25:39 (black) and 45:65 (red) for 18 different starting positions.

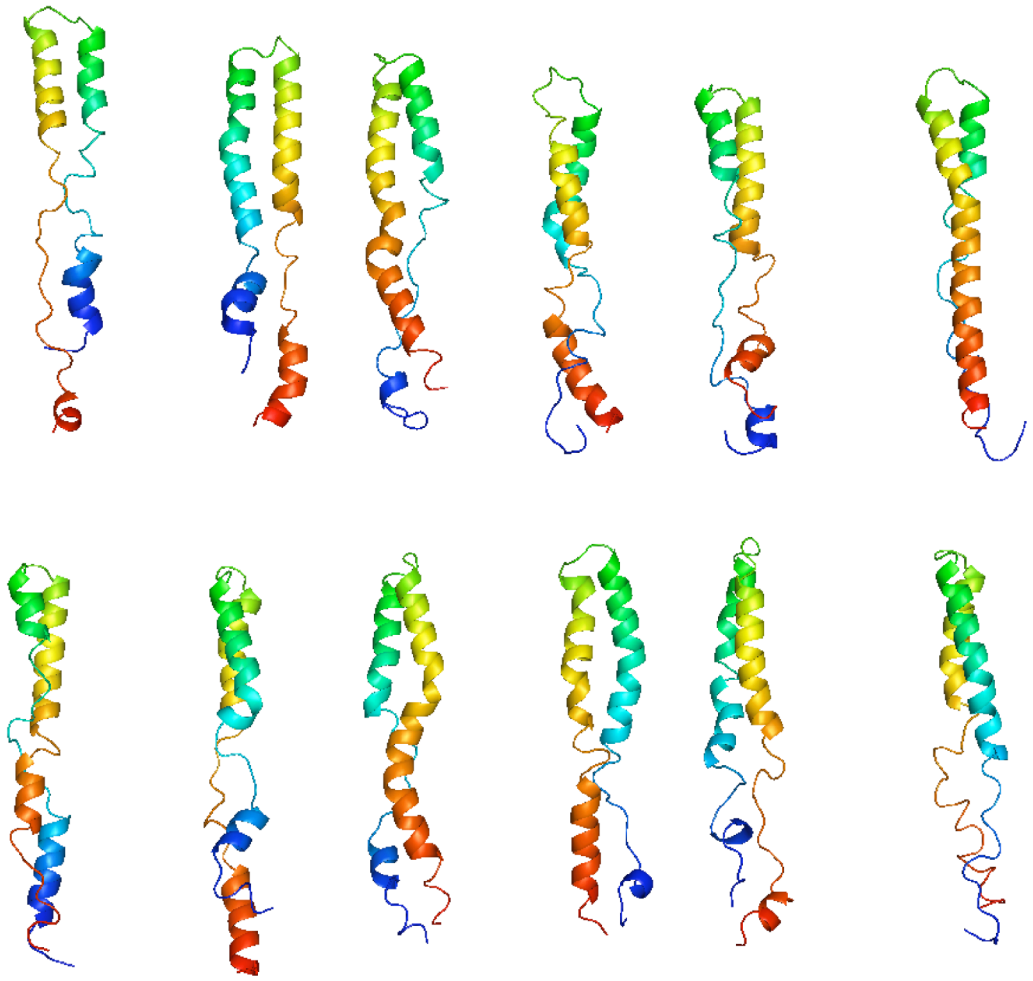

Figure S5 Conformational flexibility of the two helix bundle observed at 13.2ns corresponding to 12 different starting positions.

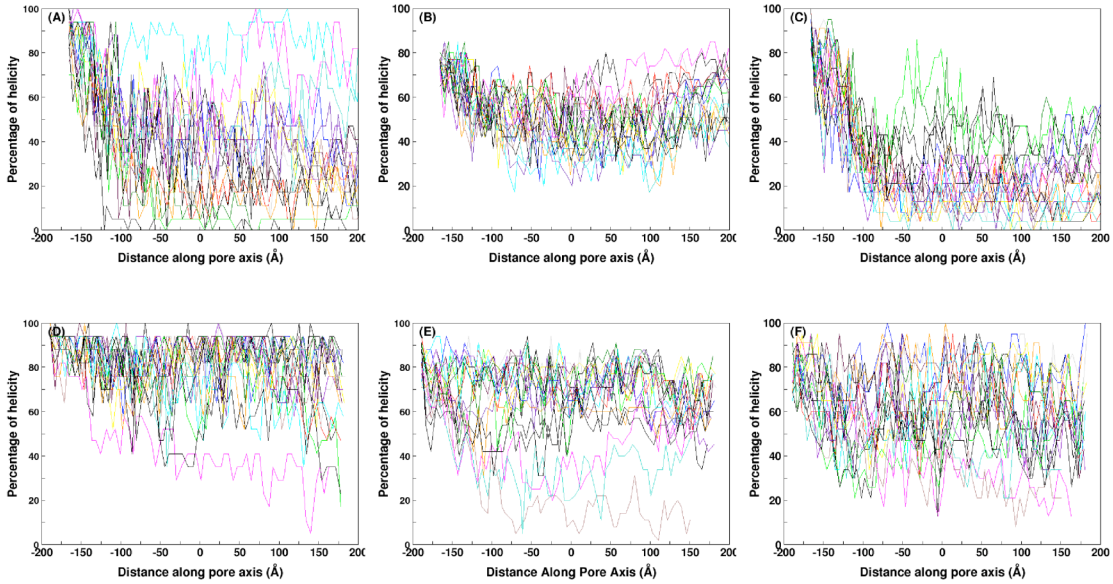

Figure S6 Percentage of helicity from individual trajectories of the pulling simulation of two helix bundle (A-C) and straight helix (D-F). Hydrogen bond distance and angle between i^{th} and $(i+4)^{th}$ residues are calculated using acceptor...hydrogen distance of 3.8Å and angle in the range of 120-180°.

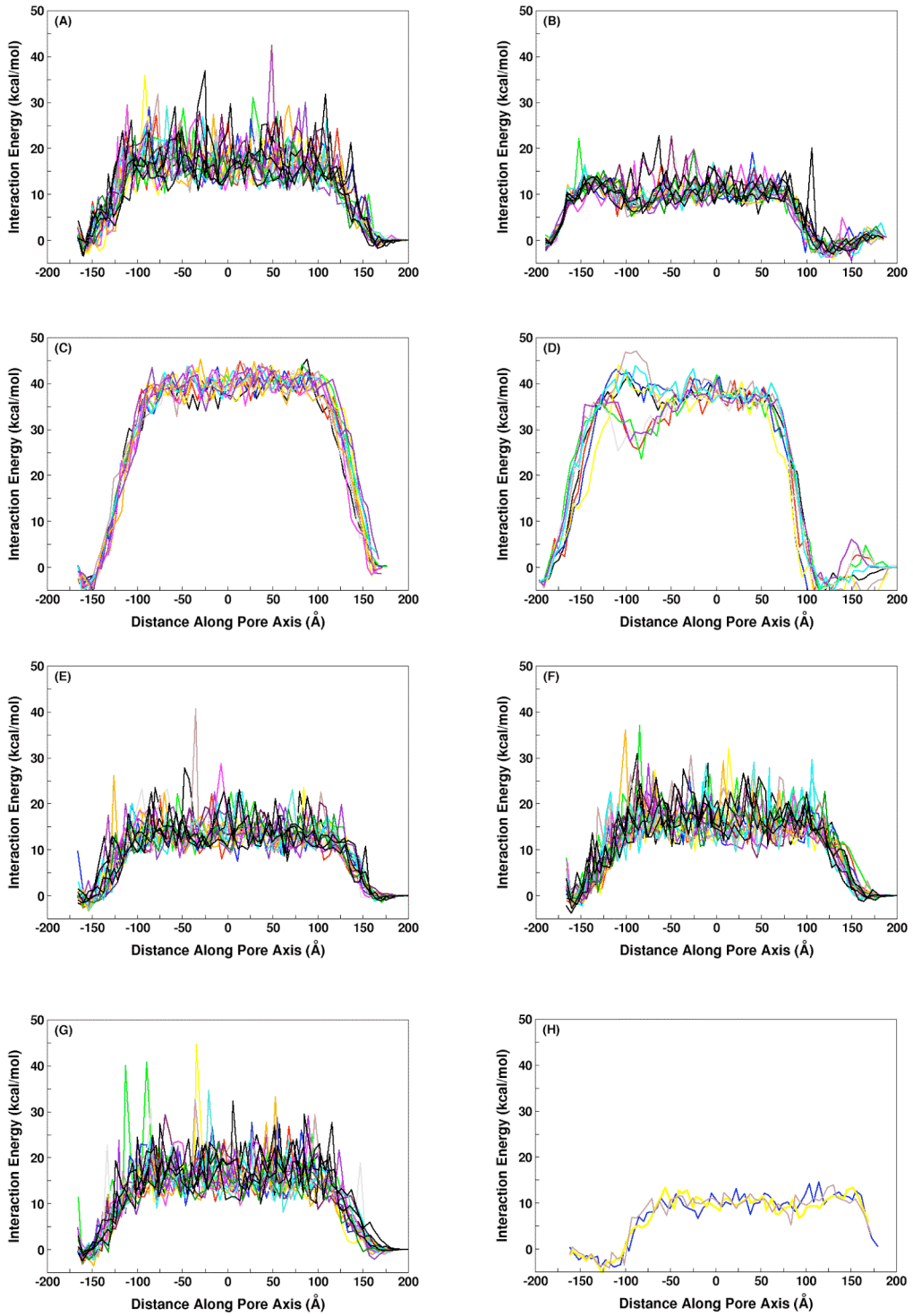

Figure S7 Interaction energy between the needle apparatus with the MxiH subunit along the pore axis for 18 different starting positions of needle with 25 Å inner diamter: wild-type (A and C) two-helix bundle and (B and D) straight helix in the presence of the salt concentration of 150mM (A and B) and 50mM (C and D) and W10A (E), W10Y (F) and W10F (G) mutants of two-helix bundle in the presence of 150mM salt concentration, (H) straight-helix with C-terminus facing inside the pore (3 different starting positions).

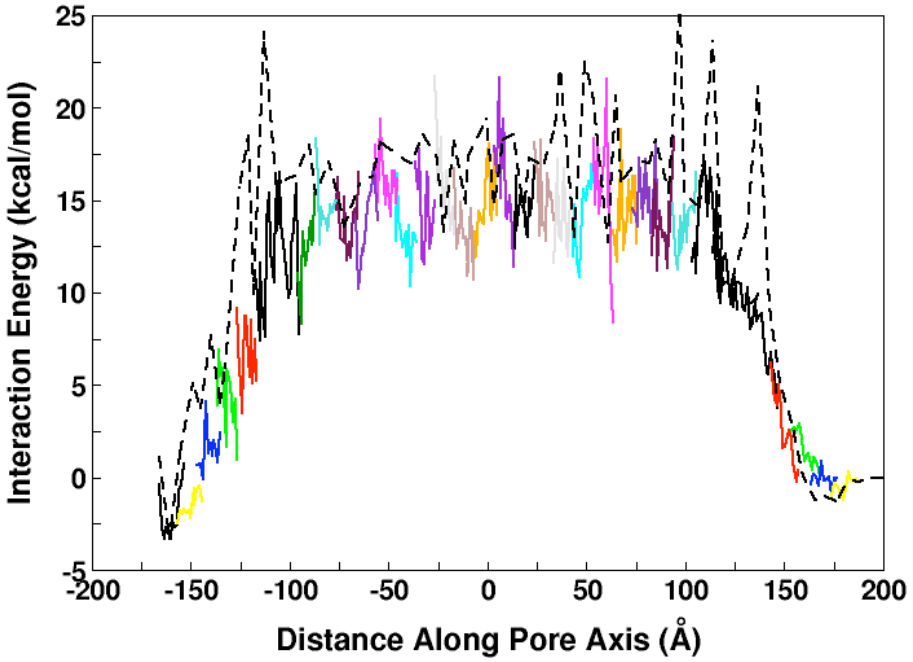

Figure S8 Interaction energy between the needle apparatus and the wild-type MxiH two-helix bundle along the pore axis of 25 Å inner diameter needle with lower pulling speed (3 Å /ns) and in the presence of the salt concentration of 150mM. Different colors of the energy profile indicate the simulation corresponding to 35 different starting conformations all along the needle channel at every 10 Å. Dotted lines correspond to the energy profile of simulation done with 15 Å /ns.

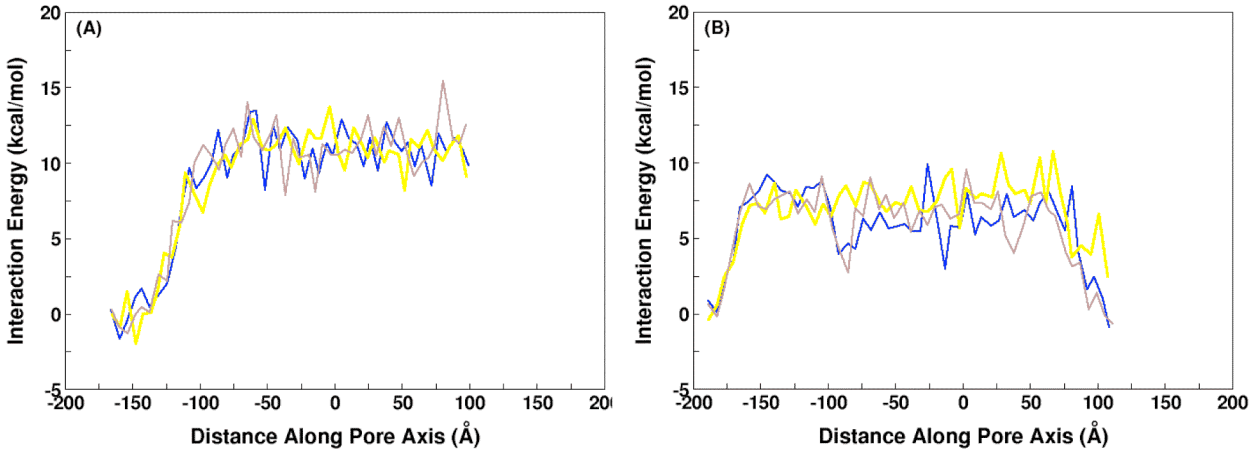

Figure S9 Interaction energy between the needle apparatus with the MxiH subunit along the pore axis for 3 different starting positions of needle with 30 Å inner diamter: wild-type (A) two-helix bundle and (B) straight helix in the presence of the salt concentration of 150mM.

Table S1 Surface electrostatics of type III secretion injectosome components and effectors from various gram negative bacteria.

Protein Name	PDB ID	Organism	pI*	Electrostatic potential **		Ref.
				Front view	Back view	
AvrB	1NH1	*P. syringae*	5.76	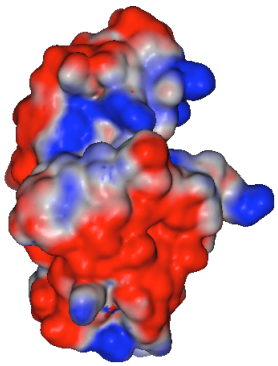	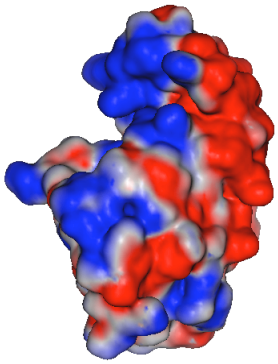	(1)
AvrPphB	1UKF	*P. syringae*	5.24	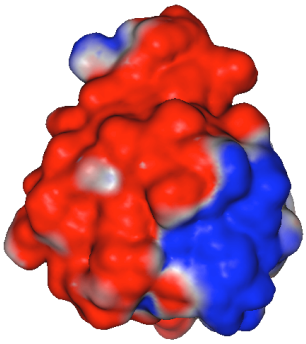	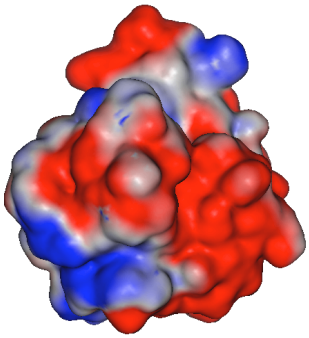	(2)
BipD	2J9T	*B. pseudomallei*	5.04	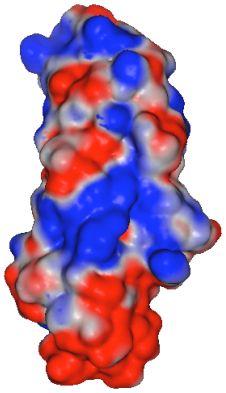	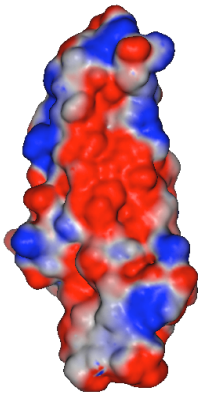	(3)

Continued ...

BsaL	2G0U	*B. pseudomallei*	5.53	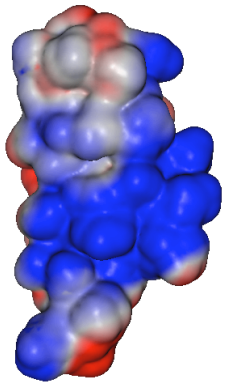	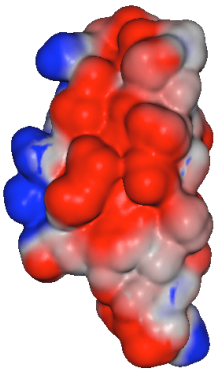	(4)
EscJ	1YJ7	*E. coli*	4.90	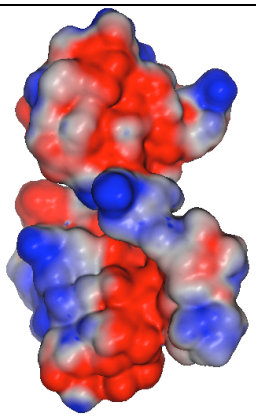	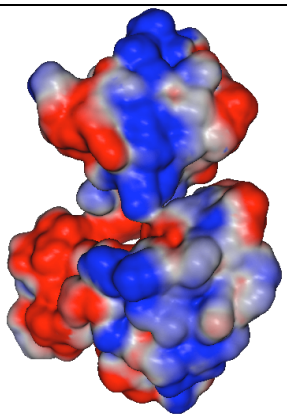	(5)
Hcv1	1Y12	*P. aeruginosa*	6.28	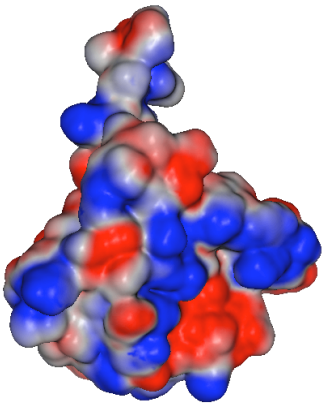	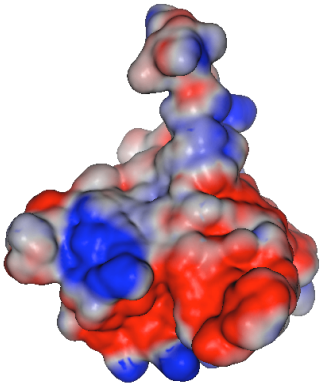	(6)
IpaD	2J0O	*S. flexneri*	5.65	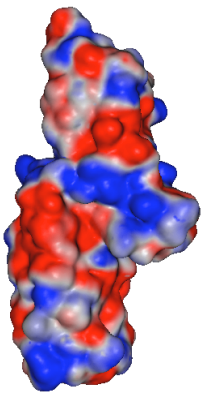	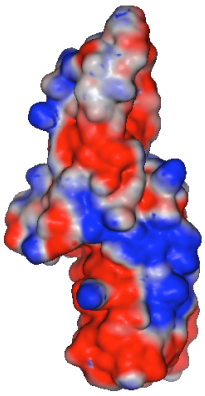	(3)

Continued …

LcrV	1R6F	*Y. pestis*	5.57	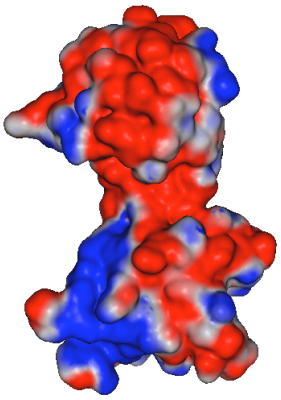	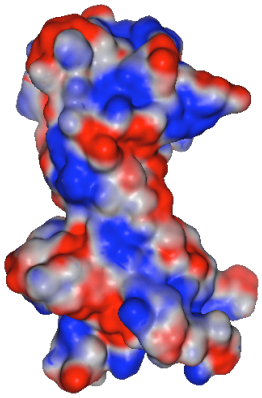	(7)
MxiH	2CA5	*S. flexneri*	4.33	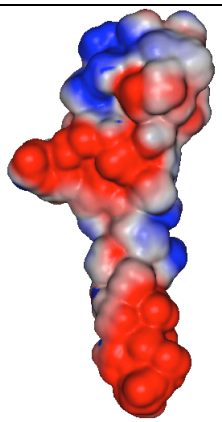	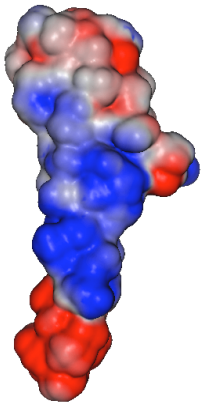	(8)
MxiM	1Y9T	*S. flexneri*	8.85	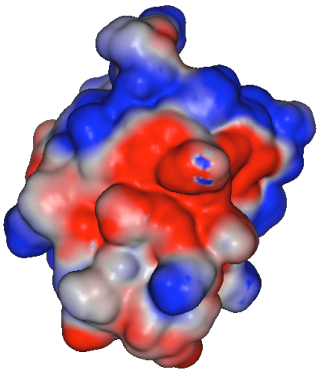	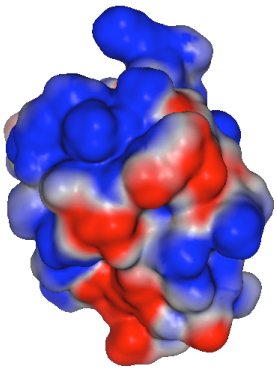	(9)
PrgI	2JOW	*S. typhimurium*	4.53	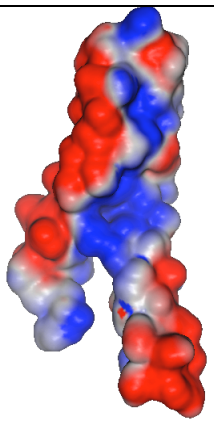	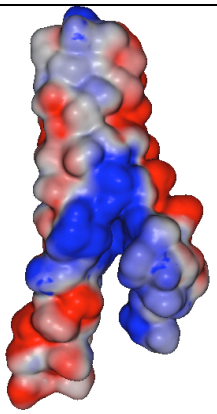	(10)

Continued …

YopH	1QZ0	*Y. pestis*	8.99	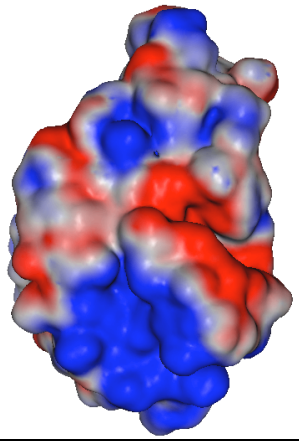	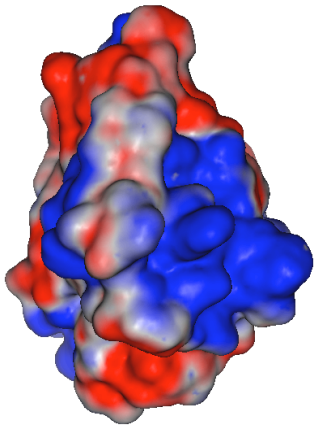	(11)

* Isoelectric point (pI) is calculated for the entire amino acid sequence.
** The electrostatic surfaces are calculated by solving PBEQ module in CHARMM (12) and its online visualization tool (13). Electrostatic scaling used for all the figures are -0.6:0 (electronegative) and 0:0.6 (electropositive). Salt concentration used for the calculation is 150mM.

References

1. Lee CC, Wood MD, Ng K, Andersen CB, Liu Y, Luginbuhl P, Spraggon G, Katagiri F (2004) Crystal structure of the type III effector AvrB from Pseudomonas syringae. *Structure* 12:487-494.
2. Zhu M, Shao F, Innes RW, Dixon JE, Xu Z (2004) The crystal structure of Pseudomonas avirulence protein AvrPphB: a papain-like fold with a distinct substrate-binding site. *Proc Natl Acad Sci U S A* 101:302-307.
3. Johnson S, Roversi P, Espina M, Olive A, Deane JE, Birket S, Field T, Picking WD, Blocker AJ, Galyov EE*, et al.* (2007) Self-chaperoning of the type III secretion system needle tip proteins IpaD and BipD. *J Biol Chem* 282:4035-4044.
4. Zhang L, Wang Y, Picking WL, Picking WD, De Guzman RN (2006) Solution structure of monomeric BsaL, the type III secretion needle protein of Burkholderia pseudomallei. *J Mol Biol* 359:322-330.
5. Yip CK, Kimbrough TG, Felise HB, Vuckovic M, Thomas NA, Pfuetzner RA, Frey EA, Finlay BB, Miller SI, Strynadka NC (2005) Structural characterization of the molecular platform for type III secretion system assembly. *Nature* 435:702-707.
6. Mougous JD, Cuff ME, Raunser S, Shen A, Zhou M, Gifford CA, Goodman AL, Joachimiak G, Ordonez CL, Lory S*, et al.* (2006) A virulence locus of Pseudomonas aeruginosa encodes a protein secretion apparatus. *Science* 312:1526-1530.
7. Derewenda U, Mateja A, Devedjiev Y, Routzahn KM, Evdokimov AG, Derewenda ZS, Waugh DS (2004) The structure of Yersinia pestis V-antigen, an essential virulence factor and mediator of immunity against plague. *Structure* 12:301-306.
8. Deane JE, Roversi P, Cordes FS, Johnson S, Kenjale R, Daniell S, Booy F, Picking WD, Picking WL, Blocker AJ*, et al.* (2006) Molecular model of a type III secretion system needle: Implications for host-cell sensing. *Proc Natl Acad Sci U S A* 103:12529-12533.
9. Lario PI, Pfuetzner RA, Frey EA, Creagh L, Haynes C, Maurelli AT, Strynadka NC (2005) Structure and biochemical analysis of a secretin pilot protein. *EMBO J* 24:1111-1121.
10. Wang Y, Ouellette AN, Egan CW, Rathinavelan T, Im W, De Guzman RN (2007) Differences in the electrostatic surfaces of the type III secretion needle proteins PrgI, BsaL, and MxiH. *J Mol Biol* 371:1304-1314.
11. Phan J, Lee K, Cherry S, Tropea JE, Burke TR, Jr., Waugh DS (2003) High-resolution structure of the Yersinia pestis protein tyrosine phosphatase YopH in complex with a phosphotyrosyl mimetic-containing hexapeptide. *Biochemistry* 42:13113-13121.
12. Brooks BR, Bruccoleri RE, Olafson BD, States DJ, Swaminathan S, Karplus M (1983) CHARMM: A Program for Macromolecular Energy, Minimization, and Dynamics Calculations. *J Comput Chem* 4:187-217.
13. Jo S, Vargyas M, Vasko-Szedlar J, Roux B, Im W (2008) PBEQ-Solver for online visualization of electrostatic potential of biomolecules. *Nucleic Acids Res* 36:W270-275.

Table S2 Surface electrostatics of propelling bacterial flagellar secretion apparatus components.

Protein Name	PDB ID	Organism	pI*	Electrostatic potential **		Ref.
				Front view	Back view	
FliC	1UCU	*S. typhimurium*	4.79			(1)
FlgE	1WLG	*S. typhimurium*	4.56			(2)
FliM	2HP7	*T. maritima*	4.47			(3)

Continued ...

FliG	1LKV	*T. maritima*	5.11	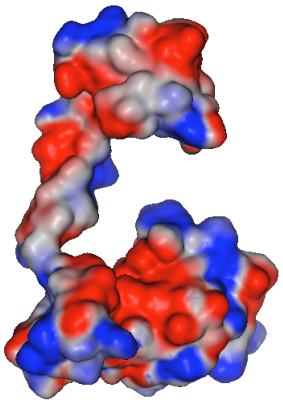	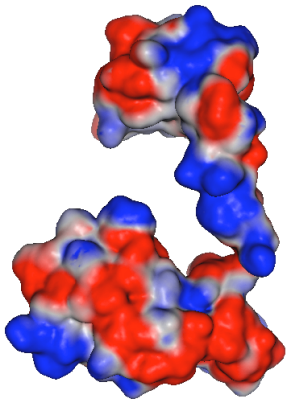	(4)
FlgK	2D4Y	*S. typhimurium*	4.64	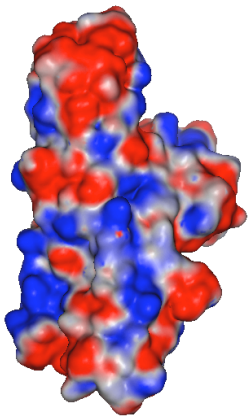	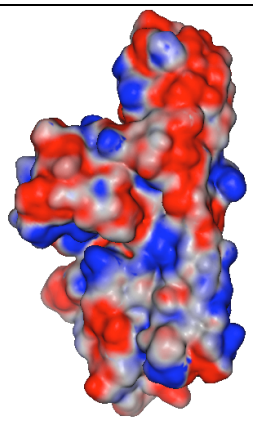	(5)
Flgl	2D4X	*S. typhimurium*	4.60	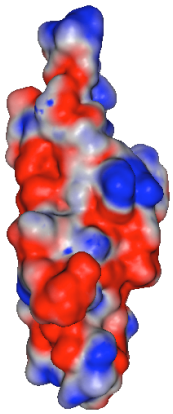	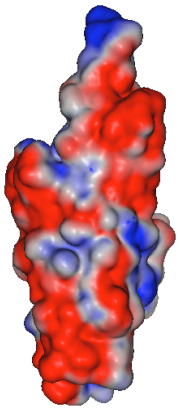	(5)

* Isoelectric point (pI) is calculated for the entire amino acid sequence.
** The electrostatic surfaces are calculated by solving PBEQ module in CHARMM (6) and its online visualization tool (7). Electrostatic scaling used for all the figures are –0.6:0 (electronegative) and 0:0.6 (electropositive). Salt concentration used for the calculation is 150mM.

References

1. Yonekura K, Maki-Yonekura S, Namba K (2003) Complete atomic model of the bacterial flagellar filament by electron cryomicroscopy. *Nature* 424:643-650.
2. Samatey FA, Matsunami H, Imada K, Nagashima S, Shaikh TR, Thomas DR, Chen JZ, Derosier DJ, Kitao A, Namba K (2004) Structure of the bacterial flagellar hook and implication for the molecular universal joint mechanism. *Nature* 431:1062-1068.
3. Park SY, Lowder B, Bilwes AM, Blair DF, Crane BR (2006) Structure of FliM provides insight into assembly of the switch complex in the bacterial flagella motor. *Proc Natl Acad Sci U S A* 103:11886-11891.
4. Brown PN, Hill CP, Blair DF (2002) Crystal structure of the middle and C-terminal domains of the flagellar rotor protein FliG. *EMBO J* 21:3225-3234.
5. Imada K, Matsunami H, Yamane M, Samatey FA, Nagashima S, Namba K Structure of the bacterial flagellar hook-filament junction *(To be Published)*.
6. Brooks BR, Bruccoleri RE, Olafson BD, States DJ, Swaminathan S, Karplus M (1983) CHARMM: A Program for Macromolecular Energy, Minimization, and Dynamics Calculations. *J Comput Chem* 4:187-217.
7. Jo S, Vargyas M, Vasko-Szedlar J, Roux B, Im W (2008) PBEQ-Solver for online visualization of electrostatic potential of biomolecules. *Nucleic Acids Res* 36:W270-275.